Nonlinear Dyn (2014) 78:1827–1837
DOI 10.1007/s11071-014-1537-4

ORIGINAL PAPER

Frequency response of primary resonance of electrostatically actuated CNT cantilevers

Dumitru I. Caruntu · Le Luo

Received: 16 September 2013 / Accepted: 3 June 2014 / Published online: 15 July 2014

Abstract This paper deals with electrostatically actuated carbon nanotube (CNT) cantilever over a parallel ground plate. Three forces act on the CNTs cantilever, namely electrostatic, van der Waals, and damping. The van der Waals force is significant for values of 50 nm or less of the gap between the CNT and the ground plate. As both forces electrostatic and van der Waals are nonlinear, and the CNTs electrostatic actuation is given by AC voltage, the CNT undergoes nonlinear parametric dynamics. The methods of multiple scales and reduced order model (ROM) are used to investigate the system under soft AC near half natural frequency of the CNT and weak nonlinearities. The frequency–amplitude response and damping, voltage, and van der Waals effects on the response are reported. It is showed that only five terms ROM predicts and accurately predicts the pull-in instability and the saddle-node bifurcation, respectively.

Keywords CNT cantilever resonators · Electrostatic actuation · Primary resonance · Frequency response

Starting fall 2015, University of Texas-Pan American becomes University of Texas-Rio Grande Valley (RGV).

D. I. Caruntu (✉)· L. Luo
Mechanical Engineering Department, University of Texas-Pan American, Edinburg, TX 78539, USA
e-mail: caruntud@utpa.edu; caruntud2@asme.org; dcaruntu@yahoo.com

1 Introduction

Since the discovery of Sumio Iijima [1] in 1991, carbon nanotubes (CNTs) became one the most widely investigated and used nano-structures. Their excellent and unique properties are worth the attention and research efforts. Several applications based on CNTs have been reported in chemistry [2–5], medicine [6–9], and mechanical engineering [10–13]. Depending on the structure of CNTs, there are two categories: single-walled carbon nano tubes (SWCNTs) [14] and multi-walled CNTs (MWCNTs) [15]. Pull-in instability in micro-electromechanical (MEMS) resonators and characteristics of the pull-in phenomenon in the presence of alternating current (AC) and direct current (DC) loads have been investigated [16]. Reduced order model (ROM) method has been used to simulate the dynamic behaviors of MEMS resonators and switches. A comprehensive nonlinear model of an electrostatically actuated clamped-clamped beam, including mechanical and electrostatic nonlinearities, valid up to displacements comparable to the gap that has been reported in the literature [17]. Mestrom et al. [18] investigated clamped–clamped beam resonator's response for various parameters. He obtained a good agreement between numerical and experiment results. Conley et al. [19] investigated the nonlinear dynamics of electrostatically actuated SWCNT resonators. It has been showed that DC bias voltages have a significant impact on the behavior of the system. They did not only tune the linear natural frequency, but also alter the qual-

itative nature of system's nonlinear response. Ouakad and Younis [20–22] reported on the variation of the natural frequency and mode shapes of clamped–clamped CNTs and focused on the forced vibration problem of CNTs actuated by AC and DC voltages. They showed that (1) transfer of energy among the vibration modes is involved in the veering phenomenon [20], the quadratic nonlinearity due to slack has a dominant effect on the dynamic behavior of the CNT [21], and subharmonic resonances are activated over a wide range of frequencies [22]. Pratiher [23] presented a study of stability and bifurcation control of ideal electrostatically actuated MEMS system. The method of multiple scales (MMS) [24] has been employed. Jia et al. [25] utilized ROM to transform the partial differential equations of motion into a system of ordinary differential equations and investigate the resonance frequency response of homogeneous and non-homogeneous micro-switches under Casimir force and applied voltage. Caruntu and Knecht [26] reported the influence of nonlinear behaviors from parametric electrostatic excitation and Casimir effect on the response of MEMS cantilevers with AC near half natural frequency. Investigations of primary resonance of other structures such as plates under electrostatic actuation are reported in the literature, Vogl and Nayfeh [27]. Regarding sensors, Kim and Lee [28] investigated nonlinear resonances of CNT with a tip mass using one-term ROM, and Nayfeh et al. [29] reported on nonlinear dynamics of resonant gas sensors. Linear and/or nonlinear beam models have been reported in the literature by Crespo da Silva and Glynn [30], Luongo et al. [31], and Luongo and Zulli [32]. Micro-/nano-structures for atomic force microscopy have been reported by Hornstein and Gottlieb [33], and Rega and Settimi [34].

In this paper, the frequency response of cantilever SWCNTs under AC electrostatic actuation near half natural frequency of the CNT is investigated. This results in primary resonance of the structure. CNTs are modeled as Euler–Bernoulli cantilevers. The electrostatic and van der Waals forces between the CNT and a parallel ground plate are soft and nonlinear. Moreover, the electrostatic force is also parametric since periodic coefficients are present in its expression. The amplitude–frequency response and influences of parameters are reported. To the best of our knowledge, this is the first time when the frequency response and effects of damping, voltage, and van der Waals forces on the response of CNT cantilevers under soft AC near half natural frequency (primary resonance), and a direct comparison between MMS and ROM, are reported. This work must be of interest to nanoelectromechanical systems (NEMS) investigators.

2 Differential equation of motion

The partial differential equation describing the motion of the CNT is given as follows, Fig. 1:

$$\rho A\frac{\partial^2 y}{\partial t^2}+EI\frac{\partial^4 y}{\partial x^4}=-b\frac{\partial y}{\partial t}+f_{elec}+f_{vdw}, \tag{1}$$

where y is the deflection of the CNT; t is time; x is the longitudinal coordinate; and ρ, A, b, E, and I are the density, cross-section area, damping coefficient, Young modulus, and cross-section moment of inertia, respectively. The forces acting on the CNT are at the right-hand side of Eq. (1), and they are damping, electrostatic f_{elec}, and van der Waals f_{vdw}. Because of the nano-scale of the structure, air is taken into account as a mechanical and viscous damper; therefore, the damping force is proportional to the deflection velocity. The electrostatic and van der Waals forces [35] are as follows:

$$f_{elec}=\frac{\pi\varepsilon_0 V_{AC}^2}{R\sqrt{\left(\frac{r}{R}\right)^2+\frac{2r}{R}}\cdot\log^2\left[1+\frac{r}{R}+\sqrt{\left(\frac{r}{R}\right)^2+\frac{2r}{R}}\right]} \tag{2}$$

$$f_{vdw}=\frac{C_6\sigma_0^2\pi^2R\sqrt{r\,(r+2R)}}{2r^5\,(r+2R)^5}\left[8r^4+32r^3R+72r^2R^2+80rR^3+35R^4\right], \tag{3}$$

where the AC voltage is given by $V_{AC}=V_0\cos\Omega t$. V_0 and Ω are the amplitude and circular frequency of the AC voltage, respectively. The constants ε_0, σ_0, and C_6 are permittivity of vacuum, graphite surface density, and a constant characterizing the interaction between two atoms [35,36]. These constants are given in Table 1. The relationship of the distances in Fig. 1 and Eqs. (2) and (3) is given as follows:

$$r=g-R-y, \tag{4}$$

where g is the gap distance between the CNT and ground plate, Fig. 1; r is the current distance between the CNT and the ground plate; R is the outer radius of the CNT; and y is the CNT deflection.

Table 1 Constants [35]

Symbol	Description	Value (unit)
ε_0	Permittivity of vacuum	$8.85*10^{12}$C^2/N/m^2
C_6	Material constant	$2.43*10^{78}$Nm^7
σ	Graphite surface density	$3.8*10^{19}$ m^{-2}
E	Young modulus	$1.2*10^{12}$ N/m^2

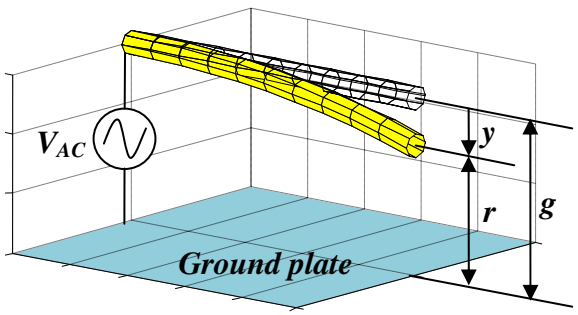

Fig. 1 CNT cantilever under electrostatic, damping, and van der Waals forces

3 Dimensionless equation of motion

The following dimensionless variables are considered:

$$w = \frac{y}{g}; \quad z = \frac{x}{\ell}; \quad \tau = \frac{t}{\ell^2}\sqrt{\frac{EI}{\rho A}}. \tag{5}$$

They are w, z, and τ dimensionless deflection, dimensionless longitudinal coordinate, and dimensionless time, respectively. Substituting Eq. (5) into Eq. (1), one obtains the boundary value problem (to include the boundary conditions) is as follows:

$$\begin{cases} \dfrac{\partial^2 w}{\partial \tau^2} + b^* \dfrac{\partial w}{\partial \tau} + \dfrac{\partial^4 w}{\partial z^4} = \delta \overline{f}_{elec} \cos^2 \Omega^* \tau + \mu \overline{f}_{vdw} \\ w(\tau, 0) = \dfrac{\partial w}{\partial z}(\tau, 0) = \dfrac{\partial^2 w}{\partial z^2}(\tau, 1) = \dfrac{\partial^3 w}{\partial z^3}(\tau, 1) = 0 \end{cases}. \tag{6}$$

Dimensionless damping b^*, dimensionless excitation (voltage) parameter δ, dimensionless actuation frequency Ω^*, and dimensionless van der Waals force parameter μ are given by

$$b^* = \frac{b\ell^2}{\sqrt{\rho A EI}}, \quad \delta = \frac{\pi \varepsilon_0 \ell^4 V_0^2}{EIg^2}$$
$$\Omega^* = \Omega \ell^2 \sqrt{\frac{\rho A}{EI}}, \quad \mu = \frac{C_6 \sigma_0^2 \pi^2 R \ell^4 g^4}{2EIg^{10}}. \tag{7}$$

The dimensionless electrostatic force $\overline{f}_{elec}$ and van der Waals force $\overline{f}_{vdw}$ in Eq. (6) are given by

$$\overline{f}_{elec} = \left[(1-w)^2 - s^2\right]^{-\frac{1}{2}} \log^{-2} \left(\frac{1-w}{s} + \sqrt{\frac{(1-w)^2}{s^2} - 1}\right) \tag{8}$$

$$\overline{f}_{vdw} = \left[(1-w)^2 - s^2\right]^{-\frac{9}{2}} \left[8g^4 (1-w-s)^4 + 32g^4 (1-w-s)^3 s + 72 g^4 (1-w-s)^2 s^2 + 80 g^4 (1-w-s) s^3 + 35 g^4 s^4\right], \tag{9}$$

where $s = R/g$

4 Method of multiple scales

The MMS is used to investigate the behavior of the system. Equations (8) and (9), and electrostatic and van der Waals forces are approximated using the first four terms of their Taylor expansions as follows:

$$\overline{f}_{elec}(w) = \sum_{k=0}^{3} \alpha_k w^k, \quad \overline{f}_{vdw}(w) = \sum_{k=0}^{3} \lambda_k w^k. \tag{10}$$

Substituting Eq. (10) into Eq. (6), one obtains

$$\frac{\partial^2 w}{\partial \tau^2} + b^* \frac{\partial^4 w}{\partial \tau} + \frac{\partial^4 w}{\partial z^4} = \mu \sum_{k=0}^{3} \lambda_k w^k + \delta \sum_{k=0}^{3} \alpha_k w^k \cos^2 \Omega^* \tau. \tag{11}$$

The system is considered to have small damping coefficient b^*, small electrostatic excitation δ, and small van der Waals parameter μ. Therefore, Eq. (11) can be written as follows:

$$\frac{\partial^2 w}{\partial \tau^2} + \varepsilon b^* \frac{\partial w}{\partial \tau} + \frac{\partial^4 w}{\partial z^4} = \varepsilon \mu \sum_{k=0}^{3} \lambda_k w^k + \varepsilon \delta \sum_{k=0}^{3} \alpha_k w^k \cos^2 \Omega^* \tau, \tag{12}$$

where ε is a bookkeeping device. Consider a first-order expansion of the deflection w and fast and slow time scales T_0, T_1 as follows:

$$w = w_0 + \varepsilon w_1, \quad T_0 = \tau, \quad T_1 = \varepsilon \tau, \tag{13}$$

where w_0, and w_1 are the zero-order and first-order approximation problems' solutions. The time derivative is then expressed in terms of derivatives with respect to the fast and slow scales

$$d/d\tau = D_0 + \varepsilon D_1, \quad D_i = d/dT_i, \quad i = 0, 1. \tag{14}$$

Substituting Eqs. (13, 14) into Eq. (12) and equate the terms of like powers of ε, one obtains the zero-order problem ε^0 and first-order problem ε^1 as follows:

$$\varepsilon^0 : D_0^2 w_0 + \frac{\partial^4 w_0}{\partial z^4} = 0 \tag{15}$$

$$\varepsilon^1 : D_1^2 w_1 + \frac{\partial^4 w_1}{\partial z^4} = -2D_0 D_1 w_0 - b^* D_0 w_0 + f\sum_{k=0}^{3} \alpha_k w^k \cos^2\left(\Omega^* \tau\right) + \mu \sum_{k=0}^{3} \lambda_k w^k. \tag{16}$$

The solution of the boundary value problem associated to the zero-order problem Eq. (15) is given by

$$w_0 = \phi_k(z)\left(Ae^{i\omega_k T_0} + \bar{A}e^{-i\omega_k T_0}\right), \tag{17}$$

where ϕ_k is the mode shape and A is a complex amplitude (depending on T_1 the slow time scale) to be determined. The kth dimensionless natural frequency ω_k and the corresponding mode shape of the uniform cantilever [26,37,38] are given by

$$\omega_k = \overline{\omega}_k \ell^2 \sqrt{\frac{\rho A}{EI}}, \quad \phi_k(z) = \cosh\left(\sqrt{\omega_k} x\right) - \cos\left(\sqrt{\omega_k} x\right) - c_k\left(\sinh\left(\sqrt{\omega_k} x\right) - \sin\left(\sqrt{\omega_k} x\right)\right), \tag{18}$$

where $\overline{\omega}_k$ is the dimensional natural frequency. The first five dimensionless natural frequencies and mode shape coefficients are given in Table 2. Substituting Eq. (17) into Eq. (16), it results in

$$D_1^2 w_1 + \frac{\partial^4 w_1}{\partial z^4} = -2\left(A' e^{i\omega_k T_0} \pm \bar{A}' e^{-i\omega_k T_0}\right)(i\omega_k)\phi_k - b^*\left(Ae^{i\omega_k T_0} - \bar{A}e^{-i\omega_k T_0}\right)(i\omega_k)\phi_k + \frac{\delta}{4}\left(e^{2i\Omega^* T_0} + 2 + e^{-2i\Omega^* T_0}\right)\left[\alpha_0 + \alpha_1\phi_k\left(Ae^{i\omega_k T_0} + \bar{A}e^{-i\omega_k T_0}\right) + \alpha_2\phi_k^2\left(A^2 e^{2i\omega_k T_0} + 2\bar{A}A + \bar{A}^2 e^{-2i\omega_k T_0}\right) + \alpha_3\phi_k^3\left(A^3 e^{3i\omega_k T_0} + 3A^2\bar{A}e^{i\omega_k T_0} + 3\bar{A}^2 A e^{-i\omega_k T_0} + \bar{A}^3 e^{-3i\omega_k T_0}\right)\right] + \mu\left[\lambda_0 + \lambda_1\phi_k\left(Ae^{i\omega_k T_0} + \bar{A}e^{-i\omega_k T_0}\right) + \lambda_2\phi_k^2\left(A^2 e^{2i\omega_k T_0} + 2\bar{A}A + \bar{A}^2 e^{-2i\omega_k T_0}\right) + \lambda_3\phi_k^3\left(A^3 e^{3i\omega_k T_0} + 3A^2\bar{A}e^{i\omega_k T_0} + 3\bar{A}^2 A e^{-i\omega_k T_0} + \bar{A}^3 e^{-3i\omega_k T_0}\right)\right]. \tag{19}$$

Solvability condition for Eq. (19) requires the right-hand side of this equation to be orthogonal to the solutions of the homogeneous equation. Therefore, multiplying the right-hand side of Eq. (19) by ϕ_k and integrate from 0 to 1, one obtains

$$-2i\omega_k g_{1kk}(A' e^{i\omega_k t_0} - \bar{A}' e^{-i\omega_k t_0}) - ib * \omega_k g_{1kk} \times (Ae^{i\omega_k t_0} - \bar{A}e^{-i\omega_k t_0}) + \frac{\delta}{4}\left(e^{2i\Omega^* T_0} + e^{-2i\Omega^* T_0} + 2\right)\left[\alpha_0 g_{0kk} + \alpha_1 g_{1kk} \times (Ae^{i\omega_k t_0} + \bar{A}e^{-i\omega_k t_0}) + \alpha_2 g_{2kk}(A^2 e^{2i\omega_k t_0} + 2A\bar{A} + \bar{A}^2 e^{-2i\omega_k t_0}) + \alpha_3 g_{3kk}(A^3 e^{3i\omega_k t_0} + 3A^2\bar{A}e^{i\omega_k t_0} + 3A\bar{A}^2 e^{-i\omega_k t_0} + \bar{A}^3 e^{-3i\omega_k t_0})\right] + \mu\left[\lambda_0 g_{0kk} + \lambda_1 g_{1kk}(Ae^{i\omega_k t_0} + \bar{A}e^{-i\omega_k t_0}) + \lambda_2 g_{2kk}(A^2 e^{2i\omega_k t_0} + 2A\bar{A} + \bar{A}^2 e^{-2i\omega_k t_0}) + \lambda_3 g_{3kk}(A^3 e^{3i\omega_k t_0} + 3A^2\bar{A}e^{i\omega_k t_0} + 3A\bar{A}^2 e^{-i\omega_k t_0} + \bar{A}^3 e^{-3i\omega_k t_0})\right] = 0, \tag{20}$$

where

$$g_{ikk} = <\phi_k^i, \phi_k> = \int_0^1 \phi_k^{i+1}(z)\, dz. \tag{21}$$

The secular terms $(e^{i\omega_k T_0})$ are eliminated from Eq. (20), resulting

Table 2 First five dimensionless natural frequencies and mode shape coefficients for CNTs

	$k=1$	$k=2$	$k=3$	$k=4$	$k=5$
ω_k	3.51602	22.0345	61.70102	120.91202	199.85929
c_k	−0.734	−1.0185	−0.9992	−1.00003	−1.00000

$$
\begin{aligned}
&-2i\omega_k g_{1kk} A' - ib * \omega_k g_{1kk} A \\
&+\frac{\delta}{4} \cdot 2\left[\alpha_1 g_{1kk} A + 3\alpha_3 g_{3kk} A^2 \bar{A}\right] \\
&+\mu\left[\lambda_1 g_{1kk} A + \lambda_3 g_{3kk} A^2 \bar{A}\right] \\
&+\text{“}other\ secular\ terms''=0
\end{aligned} \tag{22}
$$

The given terms in Eq. (22) come from all terms in Eq. (25) except the ones multiplied by $e^{2i\Omega T_0}+e^{-2i\Omega T_0}$. The “*other secular terms*” come from the terms resulting from multiplying the first bracketed expression of Eq. (19) by $e^{2i\Omega T_0}+e^{-2i\Omega T_0}$. This multiplication leads to

$$
\begin{aligned}
&\frac{\delta}{4}\Big\{\alpha_0 g_{0kk}(e^{2i\Omega T_0}+e^{-2i\Omega T_0})+\alpha_1 g_{1kk}(Ae^{i(\omega_k+2\Omega)T_0} \\
&+Ae^{i(\omega_k-2\Omega)T_0}+\bar{A}e^{-i(\omega_k-2\Omega)T_0}+\bar{A}e^{-i(\omega_k-2\Omega)T_0}) \\
&+\alpha_2 g_{2kk}\Big(A^2 e^{2i(\omega_k+\Omega)T_0}+2A\bar{A}e^{2i\Omega T_0}+\bar{A}e^{-2i(\omega_k-\Omega)T_0} \\
&+A^2 e^{2i(\omega_k-\Omega)T_0}+2A\bar{A}e^{-2i\Omega T_0}+\bar{A}^2 e^{-2i(\omega_k+\Omega)T_0}\Big) \\
&+\alpha_3 g_{3kk}\Big[A^3 e^{i(3\omega_k+2\Omega)T_0}+3A^2\bar{A}e^{i(\omega_k+2\Omega)T_0} \\
&+3A\bar{A}^2 e^{-i(\omega_k-2\Omega)T_0}+\bar{A}^3 e^{-i(3\omega_k-2\Omega)T_0} \\
&+A^3 e^{i(3\omega_k-2\Omega)T_0}+3A^2\bar{A}e^{i(\omega_k-2\Omega)T_0} \\
&+3A\bar{A}^2 e^{-i(\omega_k+2\Omega)T_0}+\bar{A}^3 e^{-i(3\omega_k+2\Omega)T_0}\Big]\Big\}=0.
\end{aligned} \tag{23}
$$

The “*other secular terms*” from among the the terms of expression (23) are to be found in the next section, where the AC frequency is considered near half natural frequency of the CNT structure.

5 AC near half natural frequency actuation

The frequency of AC actuation is near half natural frequency $\Omega \cong \omega_k/2$. This can be written as

$$
\Omega = \frac{\omega_k}{2}+\varepsilon\sigma, \tag{24}
$$

where σ is a detuning parameter and $\Omega T_0 = \omega_k T_0/2+\sigma T_1$. One can notice from Eqs. (20) and (24) that although AC is near half natural frequency, the frequency of the electrostatic force is near natural frequency, which results into primary resonance. In this case, the “*other secular terms*” from among the terms of expression (23) are given by

$$
\begin{aligned}
&\frac{\delta}{4}\left(\alpha_0+\alpha_2 g_{2kk} 2\bar{A}A\right)e^{2i\Omega^* T_0}+\frac{\delta}{4}\left(\alpha_2 g_{2kk} A^2\right) \\
&\times e^{-2i\Omega^* T_0+2i\omega_k T_0},
\end{aligned} \tag{25}
$$

including the other secular terms given by Eq. (25) into Eq. (22); the solvability condition for primary resonance (AC near half natural frequency) becomes

$$
\begin{aligned}
&-2A'\,(i\omega_k)\,g_{1kk} - b^* A\,(i\omega_k)\,g_{1kk} \\
&+\frac{\delta}{2}\left(\alpha_1 A g_{1kk}+\alpha_3 g_{3kk} 3A^2\bar{A}\right) \\
&+\mu\left(\lambda_1 A g_{1kk}+\lambda_3 g_{3kk} 3A^2\bar{A}\right) \\
&+\frac{\delta}{4}\left(\alpha_2 g_{2kk} A^2\right)e^{-2i\Omega^* T_0+2i\omega_k T_0} \\
&+\frac{\delta}{4}\left(\alpha_0+\alpha_2 g_{2kk} 2\bar{A}A\right)e^{2i\Omega^* T_0}=0.
\end{aligned} \tag{26}
$$

Consider the complex amplitude A as follows:

$$
A=\frac{1}{2}ae^{i\beta}, \tag{27}
$$

where a is a real amplitude and β is the phase. Substituting Eqs. (24) and (27) into Eq. (26), it results

$$
\begin{aligned}
&-2\left(\frac{1}{2}a'e^{i\beta}+\frac{1}{2}ae^{i\beta}i\beta'\right)(i\omega_k)\,g_{1kk} \\
&-b^*\frac{1}{2}ae^{i\beta}\,(i\omega_k)\,g_{1kk} \\
&+\frac{\delta}{2}\left(\alpha_1\frac{1}{2}ae^{i\beta}g_{1kk}+\alpha_3 g_{3kk}\frac{3}{8}a^3 e^{i\beta}\right) \\
&+\mu\left(\lambda_1\frac{1}{2}ae^{i\beta}g_{1kk}+\lambda_3 g_{3kk}\frac{3}{8}a^3 e^{i\beta}\right) \\
&+\frac{\delta}{4}\left(\alpha_2 g_{2kk}\frac{1}{4}a^2\right)e^{2i\beta-i\sigma T_1} \\
&+\frac{\delta}{4}\left(\alpha_0 g_{0kk}+\alpha_2 g_{2kk}\frac{1}{2}a^2\right)e^{i\sigma T_1}=0
\end{aligned} \tag{28}
$$

Dividing Eq. (28) by $e^{i\beta}$, one obtains

$$
\begin{aligned}
&\left(-a'-ai\beta'\right)(i\omega_k)\,g_{1kk} - b^*\frac{1}{2}a\,(i\omega_k)\,g_{1kk} \\
&+\frac{\delta}{2}\left(\alpha_1\frac{1}{2}ag_{1kk}+\alpha_3 g_{3kk}\frac{3}{8}a^3\right) \\
&+\mu\left(\lambda_1\frac{1}{2}ag_{1kk}+\lambda_3 g_{3kk}\frac{3}{8}a^3\right) \\
&+\frac{\delta}{16}\left(\alpha_2 g_{2kk}a^2\right)e^{i\beta-i\sigma T_1} \\
&+\frac{\delta}{4}\left(\alpha_0 g_{0kk}+\alpha_2 g_{2kk}\frac{1}{2}a^2\right)e^{i\sigma T_1-i\beta}=0
\end{aligned} \tag{29}
$$

A new variable γ is considered as follows:

$$
\gamma=\sigma T_1-\beta \tag{30}
$$

The real and imaginary parts are set to zero in Eq. (29). Therefore, the phase–amplitude equations describe the behavior of the system when the AC frequency is near half natural frequency (primary resonance) of the resonator and they are given by

$$a' = -\frac{b^*}{2}a + \frac{\delta}{\omega_k}\left(\alpha_2 \frac{g_{2kk}}{g_{1kk}}\frac{1}{16}a^2 + \alpha_0 \frac{1}{4}\frac{g_{0kk}}{g_{1kk}}\right)\sin\gamma \tag{31}$$

$$\begin{aligned}\gamma' = \sigma &+ \frac{\delta}{\omega_k}\left(\alpha_1\frac{1}{4} + \alpha_3\frac{g_{3kk}}{g_{1kk}}\frac{3}{16}a^2\right)\\ &+\frac{\mu}{\omega_k}\left(\lambda_1\frac{1}{2} + \lambda_3\frac{g_{3kk}}{g_{1kk}}\frac{3}{8}a^2\right)\\ &+\frac{\delta}{\omega_k}\alpha_2\frac{g_{2kk}}{g_{1kk}}\frac{1}{16}a\cos\gamma\\ &+\frac{\delta}{\omega_k}\left(\frac{\alpha_0}{4}\frac{g_{0kk}}{g_{1kk}a} + \alpha_2\frac{g_{2kk}}{g_{1kk}}a\frac{1}{8}\right).\end{aligned} \tag{32}$$

The steady-state solutions $\left(a' = \gamma' = 0\right)$ in this case result from Eqs. (31) and (32) as follows:

$$a = \frac{2}{b^*}\frac{\delta}{\omega_k}\left(\alpha_2\frac{g_{2kk}}{g_{1kk}}\frac{1}{16}a^2 + \alpha_0\frac{1}{4}\frac{g_{0kk}}{g_{1kk}}\right)\sin\gamma \tag{33}$$

$$\begin{aligned}\sigma = &-\frac{\delta}{\omega_k}\left(\alpha_1\frac{1}{4} + \alpha_3\frac{g_{3kk}}{g_{1kk}}\frac{3}{16}a^2\right)\\ &-\frac{\mu}{\omega_k}\left(\lambda_1\frac{1}{2} + \lambda_3\frac{g_{3kk}}{g_{1kk}}\frac{3}{8}a^2\right)\\ &-\frac{\delta}{\omega_k}\alpha_2\frac{g_{2kk}}{g_{1kk}}\frac{1}{16}a\cos\gamma\\ &\frac{\delta}{\omega_k}\left(\frac{\alpha_0}{4}\frac{g_{0kk}}{g_{1kk}a} + \alpha_2\frac{g_{2kk}}{g_{1kk}}a\frac{1}{8}\right).\end{aligned} \tag{34}$$

6 Reduced order model method

In order to use ROM method, the Taylor expansions of Eqs. (8) and (9) are given in the denominators. Therefore, Eq. (6) becomes

$$\frac{\partial^2 w}{\partial\tau^2} + b^*\frac{\partial w}{\partial\tau} + \frac{\partial^4 w}{\partial z^4} = \frac{\delta\cos^2\Omega^*\tau}{\sum_{k=0}^{7} a_k w^k} + \frac{\mu}{\sum_{k=0}^{7} b_k w^k}. \tag{35}$$

The ROM solution of Eq. (35) is assumed as:

$$w = \sum_{j=1}^{N} u_j(\tau)\,\phi_j(z), \tag{36}$$

where u_j is the jth variable depending on time, N is the number of the ROM terms, and ϕ_j is the jth mode shape of the cantilever. Multiplying Eq. (35) by the denominators of electrostatic force and van der Waals force, and using Eq. (36) and the following equations

$$\begin{aligned}&\frac{\partial^2 w}{\partial\tau^2} = \sum_{j=1}^{N}\ddot{u}_j(\tau)\,\phi_j(z), \quad \frac{\partial w}{\partial\tau} = \sum_{j=1}^{N}\dot{u}_j(\tau)\,\phi_j(z),\\ &\frac{\partial^4 w}{\partial z^4} = \sum_{j=1}^{N}\omega_j^2 u_j(\tau)\,\phi_j(z),\end{aligned} \tag{37}$$

then Eq. (35) becomes

$$\begin{aligned}&\left(a_0b_0 + \sum_{p=1}^{7}\sum_{i=1}^{p} a_i\lambda_{p-i}\sum_{j1,j2,\ldots,j(p-i)}^{N} u_{j1}u_{j2}\ldots u_{j(p-i)}\right.\\ &\times\phi_{j1}\phi_{j2}\ldots\phi_{j(p-i)} + \sum_{p=1}^{7}\sum_{i=p}^{7} a_i b_{7+p-i}\\ &\left.\sum_{j1,j2,\ldots,j(p+7)}^{N} u_{j1}u_{j2}\ldots u_{j(p+7)}\phi_{j1}\phi_{j2}\ldots\phi_{j(p+7)}\right)\cdot\\ &\left(\sum_{n,j}^{N}\ddot{u}_j\phi_n\phi_j + b^*\sum_{n,j}^{N}\dot{u}_j\phi_n\phi_j + \sum_{n,j}^{N}\omega_j^2 u_j\phi_n\phi_j\right)\\ &= \sum_{p=0}^{7}\left(a_p\delta\cos^2\Omega^*\tau + \mu b_p\right)\\ &\sum_{n,j1,j2,\ldots,jp}^{N} u_{j1}u_{j2}\ldots u_{jp}\phi_n\phi_{j1}\phi_{j2}\ldots\phi_{jp}.\end{aligned} \tag{38}$$

Multiplying Eq. (38) by $\phi_n(\tau)$ on both sides, integrating the equation from 0 to 1, and using the orthonormality property given by

$$\int_0^1 \phi_n\phi_j dz = \begin{cases} 0 & n \neq j \\ 1 & n = j \end{cases}, \tag{39}$$

the ROM ordinary differential equations result as follows:

$$\begin{aligned}&\left(a_0b_0g_n + \sum_{p=1}^{7}\sum_{i=1}^{p} a_i b_{p-i}\sum_{n,j1,j2,\ldots,j(p-i)}^{N} u_{j1}u_{j2}\ldots.\right.\\ &u_{j(p-i)}h_{n,j1,j2,\ldots,j(p-i)} + \sum_{p=1}^{7}\sum_{i=p}^{7} a_i b_{7+p-i}\\ &\left.\times\sum_{j1,j2,\ldots,j(p+7)}^{N} u_{j1}u_{j2}\ldots u_{j(p+7)}h_{n,j1,j2,\ldots,j(p+i)}\right)\cdot\end{aligned}$$

$$\left(\sum_{j1}^{N}\ddot{u}_{j1}+b^{*}\sum_{j1}^{N}\dot{u}_{j1}+\sum_{j1}^{N}\omega_{j1}^{2}u_{j1}\right)$$
$$=\sum_{p=0}^{7}\left(a_{p}\delta\cos^{2}\Omega^{*}\tau+\mu b_{p}\right)$$
$$\times\sum_{n,j1,j2,\ldots,jp}^{N}u_{j1}u_{j2}\ldots u_{jp}h_{n,j1,j2,\ldots jp} \quad (40)$$

where $n = 1,2,\ldots,N$, and

$$h_{n,j1,j2,\ldots,jp}=\int_{0}^{1}\phi_{n}\phi_{j1}\phi_{j2}\ldots\phi_{jp}dz \quad (41)$$

7 Numerical simulations

Numerical simulations have been conducted using MMS and ROM method. A comparison between the two methods is discussed, and conclusions are drawn. The ROM system of non-explicit-coupled differential equations given by Eqs. (40) has been solved using AUTO 07P a continuation and bifurcation software for ordinary differential equations. Meanwhile, the results of two (2T), three (3T), four (4T), and five (5T) terms ROM are also compared and showed to indicate convergence of the ROM. Table 3 gives the dimensional parameters of the system. With these parameters, the dimensionless parameters are calculated and presented in Table 4. Taylor coefficients of Eqs. (10) and (35) are given in Tables 5 and 6.

Figure 2 shows the amplitude–frequency response of CNTs under AC near half natural frequency, which results in primary resonance, using MMS and 5T ROM. Four terms of Taylor expansions in the numerators are used for MMS, and seven terms of Taylor expansions in denominators are used in the ROM in

Table 3 Dimensional parameters of the system

Symbol	*Description*	*Value (unit)*
ℓ	Length of CNT	$200*10^{-9}$ m
R	CNT radius	10^{-9} m
R_{int}	CNT inner radius	$0.665*10^{-9}$ m
g	Gap CNT - plate	$20*10^{-9}$ m
	Voltage applied	$32*10^{-3}$ V

Table 4 Dimensionless system parameters

Symbol	*Description*	*Value*
δ	Electrostatic parameter	0.1902
μ	Van der Waals parameter	0.0005
b^{*}	Damping parameter	0.001

Table 5 Taylor expansion coefficients of electrostatic force and van der Waals force, Eq. (10)

Symbol	*Value*	*Symbol*	*Value*
α_0	0.0839	λ_0	0.0839
α_1	0.1321	λ_1	0.1321
α_2	0.1779	λ_2	0.1779
α_3	0.2244	λ_3	0.2244

Table 6 Denominator Taylor expansion coefficients of the electrostatic force and van der Waals force, Eq. (35)

Symbol	Value	Symbol	Value
a_0	13.586202	b_0	0.1226795
a_1	−20.99676	b_1	−0.617992
a_2	4.6816821	b_2	1.2429685
a_3	1.2246554	b_3	−1.247656
a_4	0.5279667	b_4	0.6249998
a_5	0.2830802	b_5	−0.125001
a_6	0.15756904	b_6	−0.00000049
a_7	0.10349291	b_7	−0.00000044

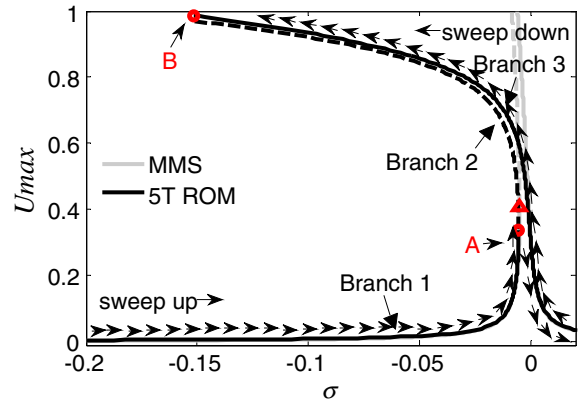

Fig. 2 Amplitude–frequency response AC near half natural frequency using MMS and seven terms denominator Taylor expansion. $b^{*} = 0.001, \delta = 0.1902$, and $\mu = 0.0005$ (◎ shows the bifurcation point at low amplitudes, and the pull-in point at high amplitudes).

order to conserve singularities. In the horizontal axis is σ the detuning dimensionless frequency, and in the vertical axis is U_{max} the amplitude of the tip of the CNT, which is the amplitude of Eq. (36) for the ROM, and the amplitude of Eq. (17) for MMS, both for $z = 1$. The ROM response shows three branches. The stable branches are showed using solid lines, and unstable branches using dash lines. When the frequency is swept up, the amplitude U_{max} of CNTs increases along branch 1 until the CNTs cantilever reaches the bifurcation point A, where a jump phenomenon occurs. The amplitude jumps upto branch 3. As the frequency continues to be swept up, the amplitude decreases along branch 3. When the frequency is swept down, the amplitude becomes larger until it reaches point B at a value of 0.98 (of the gap) at a value of the detuning parameter of -0.15. At this point, the CNT becomes unstable and goes into pull-in (contact with the ground plate). Comparing MMS and ROM, one can notice an excellent agreement between MMS and ROM for amplitudes less than 0.35 (of the gap). For larger amplitudes, MMS fails to predict the frequency response of the CNT. Caruntu et al. [37,38] showed that the ROM makes better predictions than MMS for high amplitudes for MEMS resonators. One can notice, Fig. 2, the strong softening effect in high amplitudes of the CNT predicted by ROM. MMS fails to accurately predict (1) the amplitude of the bifurcation point (0.41 by MMS and 0.34 by ROM), (2) the frequency at which pull-in occurs as sweeping down the frequency (-0.006 by MMS and -0.15 by ROM), and (3) the strong softening effect that allows for large amplitudes for detuning frequency between -0.15 and 0.

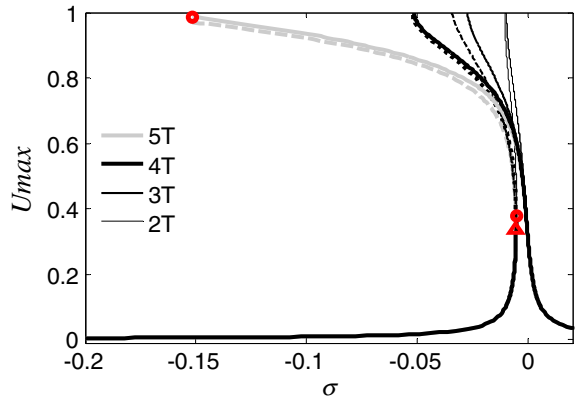

Fig. 3 ROM convergence of the amplitude–frequency response; ROM 2T, 3T, 4T and 5T. $b^* = 0.001$, $\delta = 0.1902$, $\mu = 0.0005$

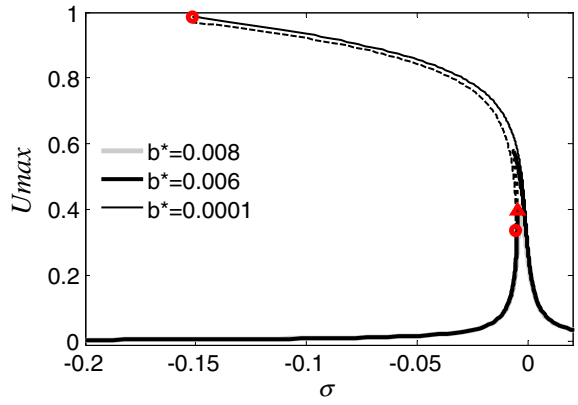

Fig. 4 Damping b^* influence on amplitude–frequency response. $\delta = 0.1902$ and $\mu = 0.0005$

8 Discussion and conclusions

In what follows the convergence of the ROM method and influences of parameters are to be discussed. Figure 3 illustrates the convergence of the ROM method. The number of terms considered in the ROM method are two, three, four, and five. One can notice the convergence of the method. As the number of the terms increases, (1) ROM better captures the strong softening (branches bent to the left) effect present in the frequency response of the electrostatically actuated CNT, and (2) the amplitude of the bifurcation point increases to 0.38. The number of terms in the ROM does not affect the predictions below an amplitude of 0.35. However, the behavior for larger amplitudes cannot be accurately predicted unless the number of terms in the ROM is five. Only five terms ROM captures the pull-in instability point B, which occurs at an amplitude of 0.98 and a detuning frequency of -0.15.

Figure 4 illustrates the influence of dimensionless damping coefficient b^* on the frequency response. As the damping increases from 0.0001 to 0.008, point B disappears becoming just a decreasing amplitude peak, preventing the system to reach pull-in. The damping parameter does not have a significant influence on the bifurcation frequency for the range of damping values considered.

Figure 5 shows the influence of dimensionless electrostatic force parameters on the frequency response. As the electrostatic parameter δ is increasing, the frequency of the bifurcation point A decreases, and its

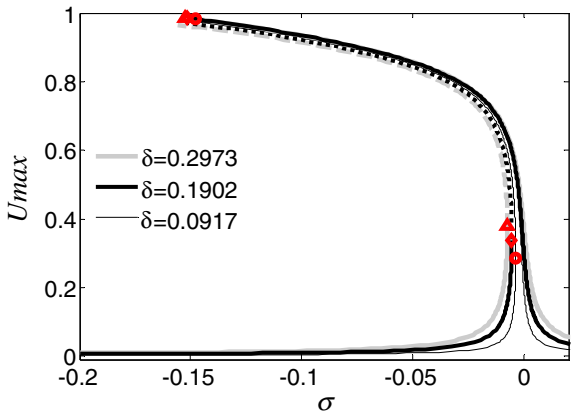

Fig. 5 Voltage parameter δ influence on amplitude–frequency response. $b^* = 0.001$, $\mu = 0.0005$, while $\delta = 0.2973$ (40 mV), $\delta = 0.1902$ (32 mV), $\delta = 0.0917$ (20 mV)

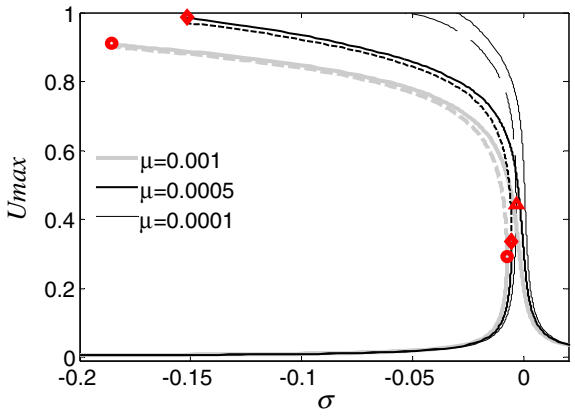

Fig. 6 van der Waals parameter μ influence on amplitude–frequency response. $\delta = 0.1902$, $b^* = 0.001$

amplitude increases. No significant differences are noticed for the amplitude of pull-in instability point B (0.98 amplitude). As the electrostatic parameter increases, the pull-in frequency of point B slightly decreases from -0.148 to -0.152.

Figure 6 illustrates the influence of the dimensionless van der Waals force parameter μ on the frequency response. As the parameter increases, (1) the softening effect becomes more significant (the branches are more bent to the left), (2) the bifurcation point A shifts to lower frequencies and amplitudes, and (3) the pull-in point B amplitude and frequency decrease.

Next, a discussion regarding the model and methods used in this work follows. Casimir force is not included in this model because it is not present for such small gaps as in this work. Casimir force and van der Waals force cannot act at the same time since they describe the same physical phenomenon at different scales (gap values) [39]. While van der Waals force models the phenomenon for gaps below 50 nm, Casimir force acts for gaps between 200 nm and 1 μm. In between is a transition between van der Waals force and Casimir force.

In this work, (a) Euler–Bernoulli continuum beam model [22,35,40–46] and (b) continuum van der Waals theory [35] for CNT resonators have been used. "Continuum models are fast and reasonably accurate for modeling and simulation" [35]. An excellent review of CNT resonators has been reported in the literature [42]. Other methods of investigation of nanotubes include 3D space-frames structures [40], nonlocal continuum mechanics (small-scale effect) [43], and molecular dynamics simulations [35]. Euler–Bernoulli model is appropriate for slender structures. If slenderness (length to diameter ratio) is greater than 20, then between CNT fundamental frequencies using Euler–Bernoulli beam theory and Timoshenko beam theory (including rotary inertia and shear deformation) is no difference [41]. Fundamental frequency is a key property of the CNT resonator; Timoshenko theory is more accurate than Euler–Bernoulli for short beams and higher modes [42]. Also, based on the concept of equivalent Euler–Bernoulli beam (equivalent rigidities), it has been reported that "the behavior of the nanotubes is length-independent except for very small lengths [40]." This was based on 3D space-frames CNT structure model. Euler–Bernoulli theory was found in good agreement with atomistic (molecular dynamics) simulations for slenderness greater than 10, Ref. [35]. It has been also reported that small-scale effect (nonlocal continuum mechanics) is not significant on the fundamental frequency for slender CNTs [43]. Classical Euler–Bernoulli fundamental frequency was found valid for slenderness greater than 20; "classical continuum models are still valid and convenient for studying vibration response of long CNTs for low modes" [43]. Continuum van der Waals theory used in this paper is in perfect agreement with the discrete Lenard–Jones potential theory. This had been showed using molecular dynamics simulations [35].

MMS is limited to weakly nonlinear systems and small amplitudes [21,26,37,38,47,48]. In this paper, we only discussed the MMS first-order uniform expansion [26,37,38,44,45] of the solution since MMS is

a perturbation method, in which "the first few steps reveal the important features of the solution and the remaining ones give small corrections," i.e., "one may calculate just few terms in a perturbation series" [49]. Regardless, the order of the MMS expansion, first-order [26,37,38,44,45], Eq. (13), or second- or third-order expansions [21], MMS fails to predict the frequency response for large amplitudes.

This paper falls in the category of analytical investigation and numerical simulations [20–22,28,29,35,39–41,43–48,50]. The results of this work are in good agreement with data reported in the literature [28,50] which showed a softening effect (saddle-node bifurcation in the lower frequency branch) of the primary resonance of electrostatically actuated CNTs. Yet, [28,50] included a significantly larger DC voltage than AC voltage, and the results were presented in dimensional form [50] rather than dimensionless which would be more general and used only one-mode approximation [28] rather than five-mode approximation which would be more accurate.

To the best of our knowledge, the present work reports for the first time a direct comparison between MMS and five terms ROM for the primary resonance of CNT cantilevers under soft AC electrostatic actuation to include the effects of damping, voltage, and van der Waals forces. It is showed that the increase of van der Waals effect results in the decrease of the amplitude and the frequency of the saddle-node bifurcation and the pull-in instability, Fig. 6. It is also showed that only five terms ROM captures both the saddle-node bifurcation and pull-in instability of the system, Fig. 3.

The limitations of this paper are as follows. First, the results are valid for slender CNT with a length to diameter ratio greater than 100 since the Euler–Bernoulli beam theory is used. Second, it does not include an experimental investigation which will be a future direction of research.

Acknowledgments This work was supported by the National Science Foundation under DMR Grant # 0934157 (PREM-The University of Texas Pan American/University of Minnesota - Science and Engineering of Polymeric and Nanoparticle-based Materials for Electronic and Structural Applications).

References

1. Iijima, S.: Helical micro-tubules of graphitic carbon. Nature **345**, 56 (1991)
2. Ren, X., Chen, C., Nagatsu, M., Wang, X.: Carbon nanotubes as adsorbents in environmental pollution management: a review. Chem. Eng. J. **170**, 395–410 (2011)
3. Groven, L.J., Puszynski, J.A.: Combustion synthesis and characterization of nickel aluminide-carbon nanotube composite. Chem. Eng. J. **183**, 515–525 (2012)
4. Li, K., Wang, W., Cao, D.: Metal (Pd, Pt)-decorated carbon nanotubes for CO and NO sensing. Sens. Actuators B Chem. **159**, 171–177 (2011)
5. Kumar, B., Castro, M., Feller, J.F.: Poly (lactic acid)-multi-wall carbon nanotube conductive biopolymer Nano composite vapor sensors. Sens. Actuators B Chem. **161**, 621–628 (2012)
6. Cheung, W., Pontoriero, F., Taratula, O., Chen, A., He, H.: DNA and carbon nanotubes as medicine. Adv. Drug. Deliv. Rev. **62**, 633–649 (2010)
7. Peretz, S., Regev, O.: Carbon nanotubes as nanocarriers in medicine. Curr. Opin. Colloid Interface Sci. **17**, 360–368 (2012)
8. Meng, L., Zhang, X., Lu, Q., Fei, Z., Dyson, P.J.: Single walled carbon nanotubes as drug delivery vehicles: targeting doxorubicin to tumors. Biomaterials **33**, 1689–1698 (2012)
9. Orynbayeva, Z., Singhal, R., Vitol, E.A., Schrlau, M.G., Papazoglou, E., Friedman, G., Gogotsi, Y.: Physiological validation of the cell health upon probing with carbon nanotube endoscope and its benefit for single-cell interrogation, Nanomedicine: Nanotechnology. Biol. Med. **8**, 590–598 (2012)
10. Aydogdu, M., Filiz, S.: Modeling carbon nanotube-based mass sensors using axial vibration and nonlocal elasticity. Physica E **43**, 1229–1234 (2011)
11. Pathangi, H., Cherman, V., Khaled, A., Soree, B., Groeseneken, G., Witvrouw, A.: Towards CMOS-compatible single-walled carbon nanotube resonators. Microelectron. Eng. **107**, 219–222 (2013)
12. Lassagne, B., Bachtold, A.: Carbon nanotube electromechanical resonator for ultrasensitive mass/force sensing. Comptes Rendus Phys. **11**, 355–361 (2010)
13. Sung, M., Paek, S., Ahn, S., Lee, J.H.: A study of carbon-nanotube-based nanoelectromechanical resonators tuned by shear strain. Comput. Mater. Sci. **51**, 360–364 (2012)
14. Lu, X., Hu, Z.: Mechanical property evaluation of single-walled carbon nanotubes by finite element modeling. Compos. B **43**, 1902–1913 (2012)
15. Georgantzinos, S.K., Anifantis, N.K.: Vibration analysis of multi-walled carbon nanotubes using a spring-mass based finite element model. Comput. Mater. Sci. **47**, 168–177 (2009)
16. Nayfeh, A.H., Younis, M.I., Abdel-Rahman, E.M.: Dynamic pull-in phenomenon in MEMS resonators. Nonlinear Dyn. **48**, 153–163 (2007)
17. Kacem, N., Hentz, S., Pinto, D., Reig, B., Nguyen, V.: Nonlinear dynamics of Nano mechanical beam resonators: improving the performance of NEMS-based sensors. Nanotechnology **20**, 275501 (2009)
18. Mestrom, R.M.C., Fey, R.H.B., van Beek, J.T.M., Phan, K.L., Nijmeijer, H.: Modeling the dynamics of a MEMs resonator: simulations and experiments. Sens. Actuators A **142**, 306–315 (2008)
19. Conley, W.G., Yu, L., Nellis, M.R., Raman, A., Krousgrill, C.M., Mohammadi, S., Rhoads, J.F.: The nonlinear dynam-

ics of electrostatically-actuated single-walled carbon nanotube. In: Proceedings of the RASD 2010 10th International conference 12–14 July, Southampton (2010)
20. Ouakad, H., Younis, M.: Natural frequencies and mode shapes of initially curved carbon nanotube resonators under electric excitation. J. Sound Vib. **330**, 3182–3195 (2011)
21. Ouakad, H.M., Younis, M.I.: Dynamic response of slacked single-walled carbon nanotube resonators. Nonlinear Dyn. **67**, 1419–1436 (2012)
22. Ouakad, H.M., Younis, M.I.: Nonlinear dynamics of electrically actuated carbon nanotube resonators. J. Comput. Nonlinear Dyn. **5**(011009), 1–13 (2010)
23. Pratiher, B.: Tuning the nonlinear behavior of resonance MEMs sensors actuated electrically. Procedia Eng. **47**, 9–12 (2012)
24. Nayfeh, A.H., Mook, D.T.: Nonlinear Oscillations. Wiley, New York (1979)
25. Jia, X.L., Yang, J., Kitipornchai, S., Lim, C.W.: Resonance frequency response of geometrically nonlinear microswitches under electrical actuation. J. Sound Vib. **331**, 3397–3411 (2012)
26. Caruntu, D.I., Knecht, M.W.: On nonlinear response near-half natural frequency of electrostatically actuated micro resonators. Int. J. Struct. Stab. Dyn. **11**(4), 641–672 (2011)
27. Vogl, G.W., Nayfeh, A.H.: Primary resonance excitation of electrically actuated clamped circular plates. Nonlinear Dyn. **47**, 181–192 (2007)
28. Kim, I.K., Lee, S.I.: Theoretical investigation of nonlinear resonances in a carbon nanotube cantilever with a tip-mass under electrostatic excitation. J. Appl. Phys. **114**, 104303 (2013)
29. Nayfeh, A.H., Ouakad, H.M., Najar, F., Choura, S., Abdel-Rahman, E.M.: Nonlinear dynamics of a resonant gas sensor. Nonlinear Dyn. **59**, 607–618 (2010)
30. Crespo da Silva, M.R.M., Glynn, C.C.: Nonlinear flexural-flexural-torsional dynamics of inextensional beams. I. Equations of motion. Mech. Based Des. Struct. Mach. **6**(4), 437–448 (1978)
31. Luongo, A., Rega, G., Vestroni, F.: On nonlinear dynamics of planar shear indeformable beams. J. Appl. Mech. **53**, 619 (1986)
32. Luongo, A., D, Zulli: Mathematical Models of Beams and Cables. Iste - Wiley, West Sussex (2013)
33. Hornstein, S., Gottlieb, O.: Nonlinear dynamics, stability and control of the scan process in noncontacting atomic force microscopy. Nonlinear Dyn. **54**, 93–122 (2008)
34. Rega, G., Settimi, V.: Bifurcation, response scenarios and dynamic integrity in a single-mode model of noncontact atomic force microscopy. Nonlinear Dyn. **73**, 101–123 (2013)
35. Dequenes, M., Rotkin, S.V., Aluru, N.R.: Calculation of pull-in voltages for carbon-nanotube-based nanoelectromechanical switches. Nanotechnology **13**, 120–131 (2002)
36. Girifalco, L.A., Hodak, M., Lee, R.S.: Carbon nanotubes, buckyballs, ropes, and a universal graphitic potential. Phys. Rev. B **62**(13), 104–110 (2000)
37. Caruntu, D.I., Martinez, I., Knecht, M.W.: ROM analysis of frequency response of AC near half natural frequency electrostatically actuated MEMS cantilevers. J. Comput. Nonlinear Dyn. **8**, 031011–1–031011–6 (2013)
38. Caruntu, D.I., Martinez, I., Taylor, K.N.: Voltage–amplitude response of alternating current near half natural frequency electrostatically actuated MEMS resonators. Mech. Res. Commun. **52**, 25–31 (2013)
39. Batra, R., Porfiri, M., Spinello, D.: Reduced-order models for microelectromechanical rectangular and circular plates incorporating the Casimir effect. Int. J. Solids Struct. **45**, 3558–3583 (2008)
40. Papanikos, P., Nikolopoulos, D.D., Tserpes, K.I.: Equivalent beams for carbon nanotubes. Comput. Mater. Sci. **43**, 345–352 (2008)
41. Hsu, J.-C., Chang, R.-P., Chang, W.-J.: Resonance frequency of chiral single-walled carbon nanotubes using Timoshenko beam theory. Phys. Lett. A **372**, 2757–2759 (2008)
42. Gibson, R.F., Ayorinde, E.O., Wen, Y.-F.: Vibrations of carbon nanotubes and their composites: a review. Compos. Sci. Technol. **67**, 1–28 (2007)
43. Wang, Q., Varadan, V.K.: Vibration of carbon nanotubes studied using nonlocal continuum mechanics. Smart Mater. Struct. **15**, 659–666 (2006)
44. Rasekh, M., Khadem, S.E.: Nonlinear vibration and stability analysis of axially loaded embedded carbon nanotubes conveying fluid. J. Phys. D: Appl. Phys. **42**, 135112 (2009)
45. Rafiee, M., Mareishi, S., Mohammadi: An investigation on primary resonance phenomena of elastic medium based single walled carbon nanotubes. Mech. Res. Commun. **44**, 51–56 (2012)
46. Hajnayeb, A., Khadem, S.E.: Nonlinear vibration and stability analysis of a double-walled carbon nanotube under electrostatic actuation. J. Sound Vib. **331**, 2443–2456 (2012)
47. Caruntu, D.I., Taylor, K.: Bifurcation type change of AC electrostatically actuated MEMS resonators due to DC voltage. Shock Vib. vol. 2014, Article ID 542023, 9 pages (2014). http://dx.doi.org/10.1155/2014/542023
48. Caruntu, D.I., Martinez, I.: Reduced order model of parametric resonance of electrostatically actuated MEMS cantilever resonators. Int. J. Non-Linear Mech. (2014). http://dx.doi.org/10.1016/j.ijnonlinmec.2014.02.007
49. Bender, C.M., Orszag, S.A.: Advanced Mathematical Methods for Scientists and Engineers. McGraw-Hill Book Company, New York (1978)
50. Ouakad, H.M., Younis, M.I.: Nonlinear dynamics of electrically actuated carbon nanotube resonators. J. Comput. Nonlinear Dyn. **5**(1), 011009 (2010)